ACERP: Vol. 3, No. 4, (Fall 2017) 34-40

Advanced Ceramics Progress

Research Article

Journal Homepage: www.acerp.ir

Enhanced Phtocatalytic Activity of α-Fe_2O_3 Nanoparticles Using 2D MoS_2 Nanosheets

P. Sangpour*, M. behtaj

Department of Nanotechnology and Advanced Materials, Materials and Energy Research Center, Karaj, Iran.

PAPER INFO

Paper history:
Received 13 March 2017
Accepted in revised form 01 July 2018

Keywords:
α-Fe_2O_3
MoS_2
Nanocomposite
Band Gap
Photocatalytic Activity

ABSTRACT

Nanocomposites of α-Fe_2O_3/MoS_2 were synthesized via hydrothermal method and characterized in terms of crystal structure, particle size, morphology, elemental purity and optical properties. Results confirmed the formation of α-Fe_2O_3/MoS_2 nanocomposites containing hematite nanoparticles with the average diameter of 40 nm and MoS_2 nanosheets with hexagonal crystal structure and sheet thickness of <10 nm. Optical band gap measurements revealed decreasing the band gap of α-Fe_2O_3 nanoparticles from 2.65 to 2.15 eV upon loading of MoS_2 nanosheets. The as-synthesized α-Fe_2O_3/MoS_2 nanocomposites showed a high absorption capability in the visible irradiation. Photocatalytic evaluations showed over 98% degradation of Rhudamine B (Rh B) organic dye within 75 minutes. Nanocomposites of α-Fe_2O_3/MoS_2 enhanced the rate of degradation as compared to the pure α-Fe_2O_3 nanoparticles and MoS_2 nanosheets.

1. INTRODUCTION

An increasing number of organic pollutants, such as different types of toxic organic dyes, are entering the water resources as a result of human industrial human [1]. Todays, many methods have been developed to eliminate these types of contaminants [2, 3]. As one of the potential solutions for solving environmental problems caused by the organic contaminants, photocatalytic degradation has attracted the attention of many researchers in recent years [4]. Therefore, a wide variety of synthetic materials has been proposed and applied for this purpose [5–11]. Metal oxide nanoparticles, such as TiO_2, ZnO, Fe_2O_3, have shown to be promising candidates for photocatalytic applications due to the favorable physicochemical and optical properties, [7–11]. Due to abundance, cheapness, non-toxicity and high stability under harsh conditions, hematite (α-Fe_2O_3) n-type semiconductor nanoparticles are regarded as the reliable photocatalysts [11, 12]. However, pure nanoparticles of hematite and general metal oxides suffer from some major weaknesses such as low photocatalytic efficiency in the visible range irradiation, low specific surface area, fast recombination, and short life span of light-generated electron-hole pairs [13–15].

*Corresponding Author's Email: Sangpour@merc.ac.ir (P. Sangpour)

Some strategies have been suggested in order to strengthen the photocatalytic performance of metal oxide nanoparticles, including doping and the load of noble metal and metal oxides [13, 15 and 16]. Although noble metals enhance the separation of electron-hole pairs, the rarity and high price of them has restricted their wider application [17]. Also, other strategies such as copolymerization, semiconductor coupling and nanostructure design of metal oxides have been adopted to strengthen the photocatalytic properties of metal oxides like hematite. However, these approaches have not had much success in increasing of photocatalytic efficiency [18]. Thus, a new and more effective approach is highly demanded to enhance the photocatalytic efficiency of metal oxides.

By the discovery of 2D graphene monolayer and its rich physical phenomenon, MoS_2, resembling graphene and a typical example of 2D layered nanomaterials, has caused great interest in the past few years [19]. As a transition metal sulfide, MoS_2 possesses many excellent properties, and its enhanced visible light absorption, proper band edge, special 2D structures, excellent mechanical and electrical properties make it an ideal candidate to form heterojunctions. Because of its narrow band gap (1.7 eV), nanoscale MoS_2 is recognized as a potential photocatalyst [1, 17]. Incorporation of MoS_2 in metal oxide nanoparticles while reducing the band gap can effectively promote transportation of electron-hole pairs generated from light emission [18, 19].

Additionally, 2D layered structure of MoS_2 contributes to the improvement of the specific surface area and good integration with oxide materials [1, 20].

Zhao et al. synthesized rhombohedron-shaped α-Fe_2O_3 nanocrystals via a facile and green hydrothermal method. The synthesized nanocrystals exhibited superior photocatalytic performance toward (Rhodamine B) RhB degradation [21]. Massey et al. prepared MoS_2 nanosheets by one-step facile and scalable hydrothermal method using polyethylene glycol as a templating material. The adsorption of RhB organic dye using as-synthesized MoS_2 nanosheets was investigated.

The results showed a high adsorption capability of about 216 $mg.g^{-1}$ that was suggested a high photocatalytic activity of MoS_2 nanosheets [22]. Wang et al. synthesized MoS_2 nanodots modified TiO_2 (P25) composite photocatalysts via a facile liquid ultrasonic mixing method. Compared to the pure P25, the MoS_2/P25 exhibited improved photocatalytic degradation activity under simulated sunlight with RhB (40 mL, 10 $mg.L^{-1}$) and the complete degradation of RhB was achieved within 20 minutes. The enhanced photocatalytic performance was attributed to the heterostructure of P25 and MoS_2 nanodots, improving their charge separation and enhancing their absorption capacity to the full sunlight spectrum [23].

Although several articles have reported the successful synthesis of heterojucions based on MoS_2 by unique photocatalytic and electrochemical properties, a few studies can realize the composite formation of 0D α-Fe2O3 nanoparicles with 2D MoS_2 nanosheets due to the lack of easy and effective ways to composite them with high performance and no agglomeration.

Based on the above considerations, α-Fe_2O_3/MoS_2 nanocomposite (FMN) has been synthesized through a facile hydrothermal reaction. Owing to some eligibility such as mild synthesis conditions, simple manipulation, optimal crystallization conditions, proper control of growth and appropriate properties of the product, the hydrothermal synthesis has been employed for synthesis of a variety of nanostructured materials [24].

Hence, hydrothermal synthesis has been chosen for synthesis of the nanoparticles in this study. The synthesized nanoparticles have been characterized in terms of crystal structure, particle size, morphology, elemental purity and optical properties by XRD, FESEM, EDS, FTIR and UV-visible absorption spectroscopy. The nanocomposite show excellent photocatalytic activity for degrading RhB, which belongs to the azo dyes family.

2. MATERIALS AND METHODS

FMN was synthesized using a two-step hydrothermal method. First, α-Fe_2O_3 nanoparticles were synthesized via a typical hydrothermal method. In detail, 2.3 g of $FeCl_3.6H_2O$ was dissolved in 60 mL deionized water. The resulting solution was poured into a 100 mL autoclave and kept in the oven at 180 ^oC for 12 h. The obtained dark brown precipitates were washed several times with deionized water and ethanol and finally dried.

For synthesis of FMN, 0.21 g of molybdenum precursor (sodium molybdate, Na_2MoO_4) dissolved in 60 ml of deionized water. Then, 0.38 g of sulfur precursor (Thiourea, H_2CSNH_2) was added to the solution under stirring on a magnetic stirrer. After that, 0.135 g of as-prepared iron oxide was added to the solution which was sonicated in an ultrasonic bath for 15 minute to form homogenous suspension.

The resulting suspension was poured in a 100 ml autoclave heated in an oven at 210 ^oC for 12 hours. After the desired time, the obtained black precipitates of Fe_2O_3-5wt%MoS_2 nanocomposite were filtered, washed several times with deionized water and ethanol and finally dried at 80 ^oC for 12 h. Also, pure MoS_2 nanosheets were synthesized using a procedure similar to the method mentioned above in absence of α-Fe_2O_3 additives.

2.1. Photodegradation of RhB

The photocatalytic activity of as-synthesized nanoparticles toward RhB was investigated at the room temperature under sun simulated irradiation. For this purpose, a 150 W xenon lamp (MAX-150, Asahi Spectra and USA) was used as the light source. For the evaluation, 50 mg of the nanoparticles were loaded into the two-wall glass reactor containing 100 ml of 25 ppm RhB aqueous solution. Then, the suspension was irradiated under visible light with the constant stirring and in a given time interval 5 ml of solution was withdrawn and centrifuged. Water circulation was used around the reaction container for keeping the temperature of solution at 25 ^oC and the schematic of setup was reported previously [31]. The concentration of RhB after each time intervals was measured at the wavelength of 554 nm by UV–visible spectrophotometer.

2.2. Characterization

X-ray diffraction (XRD) (Siemens X-30) was used to check the crystallization and crystal structure of as-synthesized nanoparticles. The morphology, particle size and elemental analysis of the nanoparticles were analyzed by the field emission scanning electron microscope (FESEM) (Tescan Mira3 LMU) equipped with Energy dispersive X-ray spectroscopy (EDS) (Quantax 200, Bruker). Fourier transform infrared spectrometer (FTIR) (Perkin Elmer Spectrum 400) was employed to investigate the functional groups of nanoparticles in the wave-number range of 400-4000 cm^{-1}. UV-visible spectrophotometer (Perkin Elmer Spectrum 400) was used to assess the optical properties and photocatalytic activity of the nanoparticles

3. RESULTS AND DISCUSSION

Fig. 1 shows the XRD patterns of as-synthesized α-Fe_2O_3 and synthesized nanocomposite. The pattern of α-Fe_2O_3 nanoparticles reveals the characteristic diffraction of (012), (104), (110), (113), (024), (116), (214) and (300) at 2θ=24.12°, 33.14°, 35.64°, 40.74°, 49.38°, 54.08°, 56.94°, 62.44°, 64.08° and 71.76°, respectively and they are assigned to the standard pure crystalline hematite (α-Fe_2O_3) phase (JCPDS 00-33-0664) [13, 14]. The XRD pattern of MoS_2 shows the diffraction peaks at 2θ=14.12°, 33.24°, 39.26° and 58.76° that are related to (002), (100), (103) and (110) crystal planes of hexagonal MoS_2 (JCPDS 01-075-1539), respectively [24, 25]. The XRD pattern of FMN shows the diffraction patterns of both α-Fe_2O_3 and MoS_2 confirming the formation of FMN. Based on Debbye-Scherrer relation, the mean crystal diameter of α-Fe_2O_3 and MoS_2 nanoparticles is calculated from the width of main diffraction planes ((104) for α-Fe_2O_3 and (002) for MoS_2) and the calculated amounts are 35 and 8 nm, respectively [14].

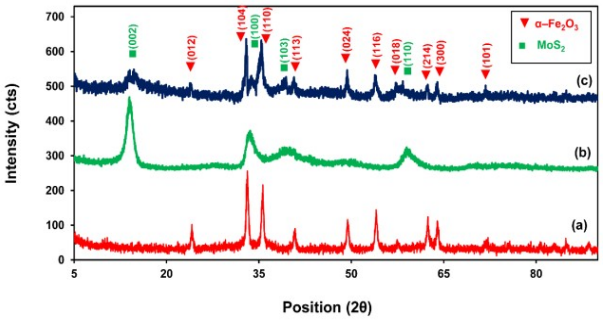

Figure 1. XRD patterns of (a): α-Fe_2O_3, (b): MoS_2 and (c): α-Fe_2O_3/MoS_2 nanoparticles

Fig. 2 shows the FESEM micrographs of as-synthesized α-Fe_2O_3, MoS_2 and FMN. This figure clearly demonstrates the formation of spherical hematite nanoparticles with the average particle size of 40 nm and MoS_2 nanosheets with the average thickness of ~10 nm.

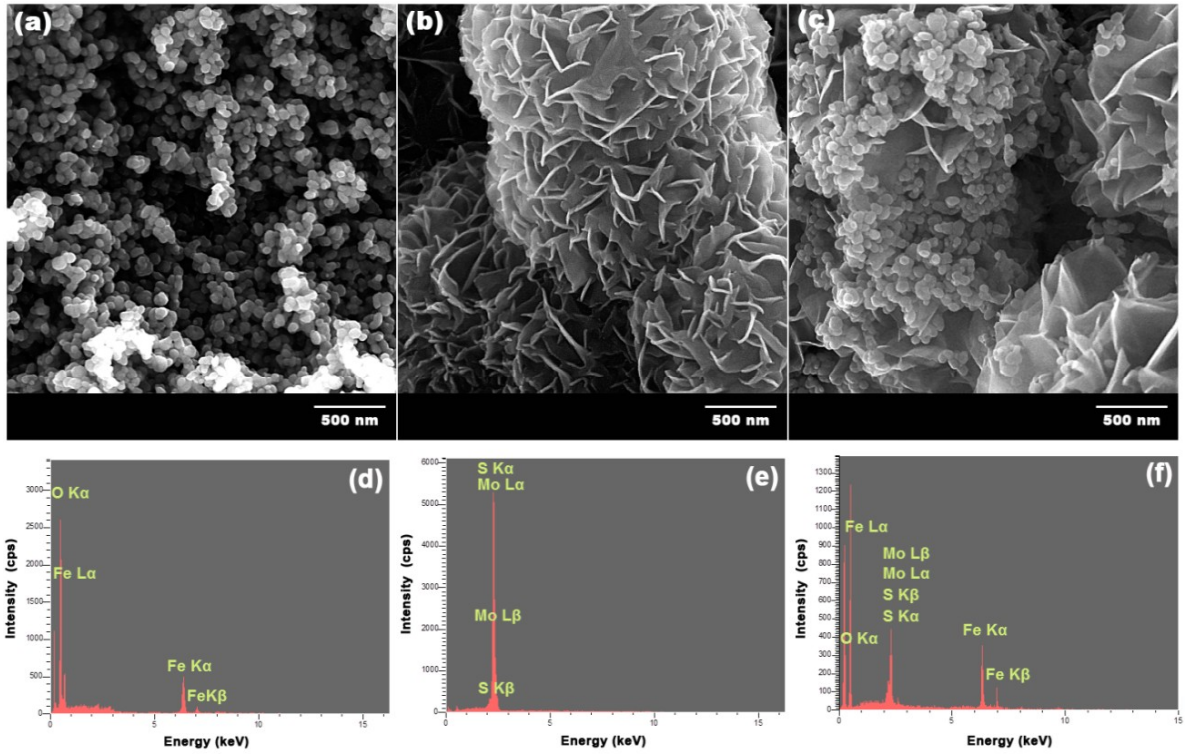

Figure 2. FESEM and EDS images of (a): α-Fe_2O_3, (b): MoS_2 and (c): α-Fe_2O_3/MoS_2 nanoparticles and EDS spectra of (d): α-Fe_2O_3, (e): MoS_2 and (f): α-Fe_2O_3/MoS_2

It is well observed that the nanoparticles are distributed on MoS_2 nanosheets implying a strong interaction between Fe_2O_3 and MoS_2 (Fig. 2c). In the hydrothermal reaction, 2D MoS_2 sheets support the Fe_2O_3 nanoparticles and facilitate the good dispersion of Fe_2O_3, which guarantee the high photocatalytic performance. The EDS patterns of as-synthesized nanoparticles clearly show they are mainly composed of Fe, O, Mo, and S (in case of α-Fe_2O_3/MoS_2). That is indicated the high elemental purity of as-synthesized nanoparticles. Based on EDS semi-quantitative data, the atomic ratios of the related elements are measured to be

2:2.92 for Fe:O (α-Fe_2O_3), 1:1.87 for Mo:S (MoS_2) and 2.04:2.96:1:1.85 for Fe:O:Mo:S (α-Fe_2O_3/MoS_2) revealing the formation of stoichiometric compounds [2, 26].

The FTIR spectra of α-Fe_2O_3 and FMN are shown in Fig. 3. A broad absorption band centered at 3467 cm^{-1} and a weak one at 1671 cm^{-1} are assigned to the stretching vibration of OH groups and bending vibration of water molecules, respectively. The weak band located at 2369 cm^{-1} reveals the presence of intercalated CO_2 species originated from atmospheric carbon dioxide [32]. Two dominant bands at 476 and 556 cm^{-1} are related to the metal-oxygen stretching vibrations (Fe-O) which confirms the presence of Fe_2O_3. The intensity of the aforementioned peaks is in the order of emphasizing the formation of α-Fe_2O_3 phase [27]. All diffraction peaks that exist in α-Fe_2O_3 and MoS_2 spectra are also found in α-Fe_2O_3/MoS_2 spectrum verifying the composite formation. Here, the characteristic peak of Mo-S bond situated at 485 cm^{-1} overlaps with Fe-O peak forming a broad peak centered at 621 cm^{-1} due to the interaction of α-Fe_2O_3 with MoS_2 [28]. In addition, the obtained small peaks at 1073, and 1436 cm^{-1} are assigned to the formation of sulfur complexes with the active sites in MoS_2 [28].

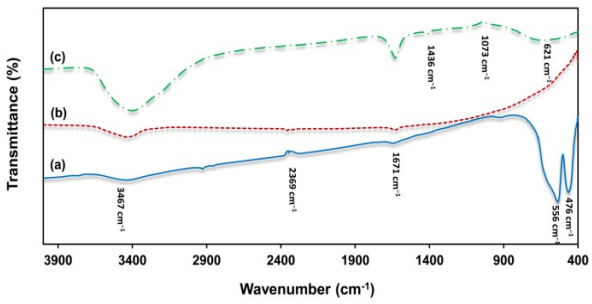

Figure 3. FTIR spectra of (a): α-Fe_2O_3, (b): MoS_2 and (c): α-Fe_2O_3/MoS_2 nanoparticles

Fig. 4(a) plotted the $(\alpha h\nu)^2$ versus $h\nu$ deduced from UV-vis absorption data to determine the band gap (E_g) value of α-Fe_2O_3, MoS_2 and α-Fe_2O_3/MoS_2 nanoparticles using Tauc's relation which is expressed by equation (1) [29]:

$$\alpha = \frac{K}{h\upsilon}(h\upsilon - E_g)^{\frac{1}{2}} \quad (1)$$

where α is the absorption coefficient (a constant that depends on the nature of the transition. Owning to the direct transition of Fe_2O_3 oxide, α=0.5 resulted in a linear relationship indicating a direct allowed optical transition thin films), h is Planck constant, ν is the transition frequency and K is the band edge constant. Therefore, by extrapolating the straight line of the plot, the values of E_g for α-Fe_2O_3, MoS_2 and FMN is measured to be 2.65, 1.86 and 2.15 eV, respectively.

These values are in good agreement with the band gap of hematite nanostructure and molybdenum sulfide nanolayer [33, 34]. The result clearly demonstrates that addition of 2D MoS_2 nanosheets to 0D α-Fe_2O_3 nanoparticles causes the narrowing of α-Fe_2O_3 band gap that is accompanied by increasing the absorption capacity in the visible region of light which has an important role in photodegradation.

Fig. 4(b) shows the degradation of RhB (Ln (C_0/C)) as a function of the irradiation time, in which C_0 and C are initial dye concentration and its concentration at time t, respectively.

For comparison, pure RhB under the visible light irradiation without catalysts were evaluated that it showed a slight degradation indicating that the photolysis mechanism of RhB can be ignored. Before light irradiation, nanostructures were stirred in dark to establish adsorption/desorption equilibrium. The result indicates that incorporation of MoS_2 significantly enhances the photocatalytic performance of α-Fe_2O_3 toward RhB photo-induced degradation. Different kinetic models have been proposed by researchers. One of the simple kinetics models is the pseudo-first order kinetic model which is expressed by equation (2) [36]:

$$\log(q_e - q_t) = \log q_e - \frac{k_1 t}{2.303} \quad (2)$$

where q_e and q_t (mg g^{-1}) are the amount of the adsorbed dye at equilibrium and at time t, respectively. k_1 (min^{-1}) is the equilibrium rate constant of pseudo-first order adsorption. By assuming the pseudo-first order kinetic of the degradation reaction, the rate constant of the reaction is calculated.

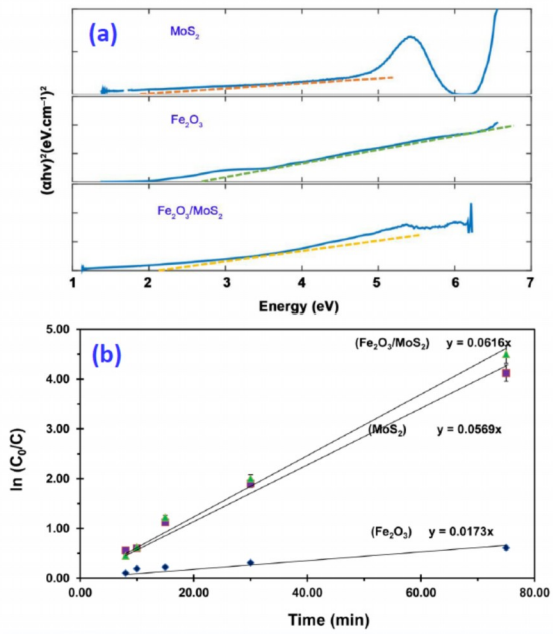

Figure 4. (a) Plot of $(\alpha h\nu)^2$ versus $h\nu$ for MoS_2 nanosheet, Fe_2O_3 nanoparticles and FMN nanocomposite and (b) The

variation of normalized $Ln(C_0/C)$ of RhB as a function of light irradiation time for MoS_2 nanosheet, Fe_2O_3 nanoparticles and FMN nanocomposite

TABLE 1. Parameters of pseudo-first order kinetic model for RhB degradation by different nanostructures

Nanostructures	Degradation Rate ($*10^{-4}$ min^{-1})	Regression coefficients (R^2)
MoS_2 nanosheet	565	0.975
Fe_2O_3 nanoparticles	173	0.971
FMN nanocomposite	616	0.938

The behavior of a semiconductor junction depends crucially on the alignment of the energy bands at the interface. Due to the more negative conduction band and valence band potential of MoS_2 than Fe_2O_3, the interface of synthesized semiconductor is a staggered gap heterojunction type. So, under the light irradiation, the photogenerated electrons and holes in the conduction band of MoS_2 transfer to the CB of Fe_2O_3 and the leaving holes will transfer from the valence band of Fe_2O_3 to the VB of MoS_2 in the opposite direction. These separations can improve the yield and lifetime of electron-hole recombination, hence the photocatalytic performance get improved (according to the proposed mechanism illustrated in Fig. 5) [35].

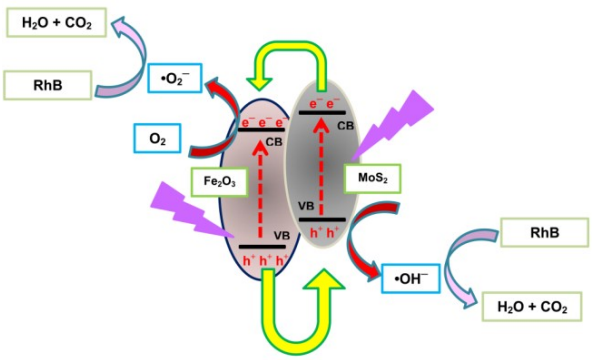

Figure 5. Schematic illustration of the RhB degradation mechanism over α-Fe_2O_3/MoS_2 nanocomposites

Migrating of carriers to the target lead to trapping of the holes by OH^- groups or H_2O to produce $OH^{\cdot}$ radicals and trapping of the electrons by the oxygen molecules to produce superoxide radical anion ($O_2^{\cdot -}$) and hydrogen peroxide radical $HO_2^{\cdot}$ [14]. In the several papers, $OH^{\cdot}$ or $HO_2^{\cdot}$ radicals have been introduced to be responsible for photodegradation of organic compounds [4, 5 and 14]. These species can attack and transform the organic molecules through the formation of intermediate compounds. In fact, $OH^{\bullet}$ radical is a strong oxidant that can very easily degrade most contaminants. Presence of O_2 may inhibit the re-combination of hole-electron pairs. Successive reactions lead to the oxidation of RhB dye and the complete photodegradation. Generally, RhB is very stable under the light irradiation when no catalyst is available. A possible mechanism for the degradation of RhB is suggested to involve three steps: 1) N-deethylation, 2) cleavage of chromophore and 3) mineralization of the dye [37]. MoS_2 nanosheets in the nanocomposite have a beneficial role. It can delay recombination rate of electron-hole pairs and enhance the photocatalytic efficiency. Therefore, addition of MoS_2 to α-Fe_2O_3 for formation of FMN can speed up the degradation of RhB to 3.56 times as compared to the pure α-Fe_2O_3 photocatalysts.

4. CONCLUDING REMARKS

Three dimentional α-Fe_2O_3 nanoparticles, 2D MoS_2 nanosheets and α-Fe_2O_3/MoS_2 nanocomposites were synthesized by the hydrothermal method. SEM results confirmed formation of hematite (α-Fe_2O_3) nanoparticles with the average size of 40 nm and MoS_2 nanosheets with the thickness <10 nm. Optical band gap analysis revealed that the addition of MoS_2 nanosheets to α-Fe_2O_3 nanoparticles caused the decrease of band gap from 2.65 to 2.15 eV enhancing the light absorption capability in the visible region. Photocatalysis measurements suggested that α-Fe_2O_3/MoS_2 nanoparticles showed higher activity in the degradation of RhB organic dye compared to pure α-Fe_2O_3 nanoparticles and MoS_2 nanosheets. Indeed, MoS_2 nanosheets and α-Fe_2O_3 nanoparticles formed heterostructures with increasing specific surface area and engineering of band gap that provide the migration of excited electrons from MoS_2 with a narrower band gap to α-Fe_2O_3 resulting in charge separation and consequently speeding up the photocatalytic degradation of RhB by α-Fe_2O_3/MoS_2 nanocomposites.

5. ACKNOWLEDGMENTS

The financial support received from Iran National Science Foundation: INSF, due 93014425 project code is acknowledged.

REFERENCES

1. Awasthi, G.P., Adhikari, S.P., Ko, S., Kim, H.J., Park, Ch.H., Kim, Ch.S., "Facile synthesis of ZnO flowers modified graphene like MoS_2 sheets for enhanced visible-light-driven photocatalytic activity and antibacterial properties", ***Journal of Alloys and Compounds***, Vol. 682, (2016), 208-215.
2. Liu, Y., Sun, L.i, Wu, J., Fang, T., Cai, R., Wei, A., "Preparation and photocatalytic activity of ZnO/Fe_2O_3 nanotube composites", ***Materials Science and Engineering: B***, Vol. 194, (2015), 9-13.
3. Guo, Sh., Zhang, G., Wang, J., "Photo-Fenton degradation of rhodamine B using Fe_2O_3-Kaolin as heterogeneous catalyst:

Characterization, process optimization and mechanism", ***Journal of Colloid and Interface Science,*** Vol. 433, (2014), 1-8.

4. Borges, M.E., Sierra, M., Méndez-Ramos, J., Acosta-Mora, P., Ruiz-Morales, J.C., Esparza, P., "Solar degradation of contaminants in water: TiO_2 solar photocatalysis assisted by up-conversion luminescent materials", ***Solar Energy Materials & Solar Cells,*** Vol. 155, (2016), 194-201.
5. Kurnianditia Putri, L.i, Tan, L.-L., Ong, W.J., Chang, W.S., Chai, S.P., "Graphene oxide: Exploiting its unique properties toward visible-light-driven photocatalysis", ***Applied Materials Today***, Vol. 4, (2016), 9-16.
6. Li, M., Huang, H.i, Yu, S., Tian, N., Dong, F., Du, X., Zhang, Y., "Simultaneously promoting charge separation and photoabsorption of BiOX (X= Cl, Br) for efficient visible-light photocatalysis and photosensitization by compositing low-cost biochar", ***Applied Surface Science***, Vol. 386, (2016), 285-295.
7. Sohrabnezhad, S., Seifi, A., "The green synthesis of Ag/ZnO in montmorillonite with enhanced photocatalytic activity", ***Applied Surface Science***, Vol. 386, (2016), 33-40.
8. Li, J., Xu, X.o, Liu, X., Yu, C., Yan, D., Sun, Z., Pan, L., "Sn doped TiO_2 nanotube with oxygen vacancy for highly efficient visible light photocatalysis", ***Journal of Alloys and Compounds***, Vol. 679, (2016), 454-462.
9. Bystrova, V.S., Piccirillo, C., Tobaldi, D.M., Castro, P.M.L., Coutinhod, J., Kopyl, S., Pullar, R.C., "Oxygen vacancies, the optical band gap (E_g) and photocatalysis of hydroxyapatite: Comparing modeling with measured data", ***Applied Catalysis B: Environmental***, Vol. 196, (2016),100-107.
10. Wang, C., Huang, Z., "Controlled synthesis of α-Fe_2O_3 nanostructures for efficient photocatalysis", ***Materials Letters***, Vol. 164, (2016), 194-197.
11. Yin, Q., Qiao, R., Zhu, L., Li, Z., Li, M., Wu, W., "α-Fe_2O_3 decorated ZnO nanorod-assembled hollow microspheres: Synthesis and enhanced visible-light photocatalysis", ***Materials Letters***, Vol. 135, (2014), 135-138.
12. Xie, J., Zhou, Z., Lian, Y., Hao, Y., Li, P., Wei, Y., "Synthesis of α-Fe_2O_3/ZnO composites for photocatalytic degradation of pentachlorophenol under UV-vis light irradiation", ***Ceramics International***, Vol. 41, (2015), 2622-2625.
13. Zhang, S., Ren, F., Wu, W., Zhou, J., Lingling, S., Xiao, X., Jiang, C., "Size effects of Ag nanoparticles on plasmon-induced enhancement of photocatalysis of Ag-α-Fe_2O_3 nanocomposites", ***Journal of Colloid and Interface Science***, Vol. 427, (2014), 29-34.
14. Wang, T., Yang, G., Liu, J., Yang, B., Ding, S., Yand, Z, Xiao, T., "Orthogonal synthesis, structural characteristics, and enhanced visible-light photocatalysis of mesoporous Fe_2O_3/TiO_2 heterostructured microspheres", ***Applied Surface Science***, Vol. 311, (2014), 314-323.
15. Liang, H., Jiang, X., Chen, W., Wang, S., Xu, B., Wang, Z., "α-Fe_2O_3/Pt hybrid nanorings and their enhanced photocatalytic activities", ***Ceramics International***, Vol. 40, (2014), 5653-5658.
16. Wei, Y., Han, S., Walker, D.A., Warren, S.C., Grzybowski, B.A., "Enhanced photocatalytic activity of hybrid Fe_2O_3-Pd nanoparticulate catalysts", ***Chemical Science,*** Vol. 3, (2012), 1090-1094.
17. Xiang, Q., Yu, J., Jaroniec, M., "Synergetic effect of MoS_2 and graphene as cocatalysts for enhanced photocatalytic H_2 production activity of TiO_2 nanoparticles", ***Journal of the American Chemical Society,*** Vol. 134, (2012), 6575-6578.
18. Liu, H., Lv, T., Zhu, C., Su, X., Zhu, Z., "Efficient synthesis of MoS_2 nanoparticles modified TiO_2 nanobelts with enhanced visible-light-driven photocatalytic activity", ***Journal of Molecular Catalysis A: Chemical***, Vol. 396, (2015), 136-142.
19. Wang, D., Xu, Y., Sun, F., Zhang, Q., Wang, P., Wang, X., "Enhanced photocatalytic activity of TiO_2 under sunlight by MoS_2 nanodots modification", ***Applied Surface Science***, Vol. 377, (2016), 221-227.
20. Zhu, C., Zhang, L., Jiang, B., Zheng, J., Hu, P., Li, S., Wu, M., Wu, W., "Fabrication of Z-scheme Ag_3PO_4/MoS_2 composites with enhanced photocatalytic activity and stability for organic pollutant degradation", ***Applied Surface Science,*** Vol. 377, (2016), 99-108.
21. Zhao, Y., Pan, F., Li, H., Niu, T., Xu, G., Chen, W., "Facile synthesis of uniform α–Fe_2O_3 crystals and their facet-dependent catalytic performance in the photo-Fenton reaction", ***Journal of Materials Chemistry A***, Vol. 1, (2013), 7242-7246.
22. Massey, A.T., Gusain, R., Kumari, S., Khatri, O.P., "Hierarchical microspheres of MoS_2 nanosheets: Efficient and regenerative adsorbent for removal of water-soluble dyes", ***Industrial and Engineering chemistry Research***, Vol. 55, (2016), 7124-7131.
23. Wang, D., Xu, Y., Sun, F., Zhang, Q., Wang, P., Wang, X., "Enhanced photocatalytic activity of TiO_2 under sunlight by MoS_2 nanodots modification", ***Applied Surface Science***, Vol. 377, (2016), 221-227.
24. Zhang, X., Huang, X., Xue, M., Ye, X., Lei, W., Tang, H., Li, C., "Hydrothermal synthesis and characterization of 3D flower-like MoS_2 microspheres", ***Materials Letters,*** Vol. 148, (2015), 67-70.
25. Qiao, X., Hu, F., Hou, D.,Li, D., "PEG assisted hydrothermal synthesis of hierarchical MoS_2 microspheres with excellent adsorption behavior", ***Materials Letters***, Vol. 169, (2016), 241-245.
26. Zhang, X., Tang, H., Xue, M., Li, C., "Facile synthesis and characterization of ultrathin MoS_2 nanosheets", ***Materials Letters***, Vol. 130, (2014), 83-86.
27. Song, H., Zhang, X., Chen, T., Jia, X., "One-pot synthesis of bundle-like β-FeOOH nanorods and their transformation to porous α-Fe_2O_3 microspheres", ***Ceramics International***, Vol. 40, (2014), 15595-15602.
28. Khawula, T.N.Y., Raju, K., Franklyn, P.J., Sigalas, I., Ozoemena, K. I., "Symmetric pseudocapacitors based on molybdenum disulfide (MoS_2)-modified carbon nanospheres: correlating physicochemistry and synergistic interaction on energy storage", ***Journal of Materials Chemistry***, Vol. 4, (2016), 6411-6425.
29. Karimi, M., Eshraghi, M.J., Jahangir, V., "A facile and green synthetic approach based on deep eutectic solvents toward synthesis of CZTS nanoparticles", ***Materials Letters,*** Vol. 171, (2016), 100-103.
30. Yuan, Y.J., Tu, J.-R., Ye, Z.J., Chen, D.Q., Hu, B., Huang, Y.-W., Chen, T.T., Cao, D.P., Yu, Z.T., Zou, Z.-G., "MoS_2-Graphene/$ZnIn_2S_4$ hierarchical microarchitectures with an electron transport bridge between light-harvesting semiconductor and cocatalyst: A highly efficient photocatalyst for solar hydrogen generation", ***Applied Catalysis B, Environmental***, Vol. 188, (2016), 13-22.
31. Farhadian, M. Sangpour, P., Hosseinzadeh, G., "Preparation and photocatalytic activity of WO_3–MWCNT nanocomposite for degradation of naphthalene under visible light irradiation", ***RSC Advances***, Vol. 6, (2016), 39063-39075.
32. Hosakun, Y., "ATR-FTIR study of the interaction of CO_2 with bacterial cellulose-based membranes", PhD Dissertation University of Sopron, (2017).
33. Misho, R.H., Murad, W.A., "Band gap measurements in thin films of hematite Fe_2O_3, pyrite FeS_2 and troilite FeS prepared by chemical spray pyrolysis", ***Solar Energy Materials and Solar Cells,*** Vol. 27, 1992, 335-345.

34. Yakovkin, I.N., "Dirac cones in graphene, Interlayer interaction in layered materials, and the band gap in MoS_2", ***Crystals,*** Vol. 6 **, (**2016), 143-156.

35. Yang, X., Sun, H., Zhang, L., Zhao, L., Lian, J., Jiang, Q., "High efficient photoFenton catalyst of α-Fe_2O_3/MoS_2 hierarchical Nanoheterostructures: Reutilization for Supercapacitors", ***Scientific Reports***, Vol. 6, (2016), 1-12.

36. Cai,W., Yu, J., Cheng, B., Su, B.L., Jaroniec, M., "Synthesis of boehmite hollow core/shell and hollow microspheres via sodium tartrate-mediated phase transformation and their enhanced adsorption performance in water treatment", ***Journal of Physical Chemistry C***, Vol. 113 (2009) 14739-14746.

37. Al-Kahtani, A. A., "Photocatalytic degradation of Rhodamine B dye in Wastewater using Gelatin/CuS/PVA nanocomposites under solar light irradiation", ***Journal of Biomaterials and Nanobiotechnology***, Vol. 8, (2017) 66-82.